Single-defect Bragg stacks for high-power narrow-band thermal emission

Philippe Ben-Abdallah and Bo Ni

Citation: Journal of Applied Physics **97**, 104910 (2005); doi: 10.1063/1.1898450
View online: http://dx.doi.org/10.1063/1.1898450
View Table of Contents: http://scitation.aip.org/content/aip/journal/jap/97/10?ver=pdfcov
Published by the AIP Publishing

Single-defect Bragg stacks for high-power narrow-band thermal emission

Philippe Ben-Abdallah[a)]
Laboratoire de Thermocinétique, Centre National de la Recherche Scientifique (CNRS), Polytechnique, Nantes Cedex 44 306, France

Bo Ni
Department of Environmental Sciences and Engineering, Dong Hua University, Shanghai 200051, China

(Received 2 September 2004; accepted 9 March 2005; published online 4 May 2005)

The radiative properties of single-defect Bragg stacks are investigated in the midinfrared region with the transfer-matrix theory. For a sufficiently small number of layers we find a regime where the structure emits radiation within a narrow range of wavelengths ($\delta\lambda/\lambda \leqslant 0.01$) and with an emissivity close to 1 in all directions. A description of the electric-field distribution inside the structure allows us to interpret this behavior in terms of coupling between the localized defect states and surface waves. This result should find broad applications in infrared spectroscopy, chemical sensing, and thermophotovoltaic conversion. © *2005 American Institute of Physics*. [DOI: 10.1063/1.1898450]

I. INTRODUCTION

Controlling the temporal coherence[1] of thermal light a hot body emits when it relaxes to lower states is undoubtedly one of the major objectives for improving the efficiency of numerous actual technologies, such as thermophotovoltaïc conversion devices, infrared spectrometers, and infrared gas sensors. Until recently thermal sources were considered as objects that were able to emit light only over a broad band of the infrared spectrum. Today, we know this paradigm is wrong,[2,3] and several partially coherent thermal sources have already been fabricated.[4,5] The physical origin of these unusual behaviors comes from the structures at the wavelength scale of materials used to fabricate these sources. They offer the potential for radically changing the way light moves through them and enables engineering of the radiative properties.[6] One of the best achievements in the design of spectrally coherent thermal sources has been obtained with photonic crystals.[7] These periodic dielectric structures, also known as photonic band gap (PBG) materials, have attracted much attention for almost two decades because of their high potentiality in numerous applied and theoretical fields (see Benisty *et al.* in Ref. 7). At sufficient refractive-index contrast, PBG materials forbid photons to propagate through them at certain frequencies, irrespective of propagation direction in space and polarization. Coupled with frequency-selective surfaces, photonic crystals have recently allowed the construction of narrow band IR emitters.[8] During these last years, promising results have opened prospects for the fabrication of temporally coherent IR sources. Indeed, when a defect is introduced into a photonic crystal it has been observed that localized electromagnetic modes could be created within the PBG.[9,10] Such defects act like waveguides with a confinement achieved by means of the photonic band gap and not by total internal reflection as in traditional waveguides. However, these mechanisms, which are well explained by lossless structures,[11,12] remain unclear when dissipation phenomena take place.[13]

II. MODEL AND SCATTERING EXPERIMENTS

Herein, we report a numerical investigation of radiative properties in the IR region of Bragg stacks with a single absorbing defect embedded within. The defect layer we consider is assumed to be plane and homogeneous. Its dielectric permittivity is described by a simple Lorentz model

$$\varepsilon_3(\omega) = \varepsilon_\infty \left[1 + \frac{\omega_L^2 - \omega_T^2}{\omega_T^2 - \omega^2 - i\Gamma\omega} \right], \tag{1}$$

where $\omega_L, \omega_T, \Gamma$, and ε_∞ denote the longitudinal and transversal optical phonon frequencies, the damping factor, and the high-frequency dielectric constant, respectively. The defect layer is symmetrically (Fig. 1) recovered on both sides by a crystal made with a small number of unit cells, themselves made with two layers of nonabsorbing materials of dielectric constant ε_1 and ε_2. Moreover, the whole structure is assumed embedded in vacuum ($\varepsilon_0 = 1$).

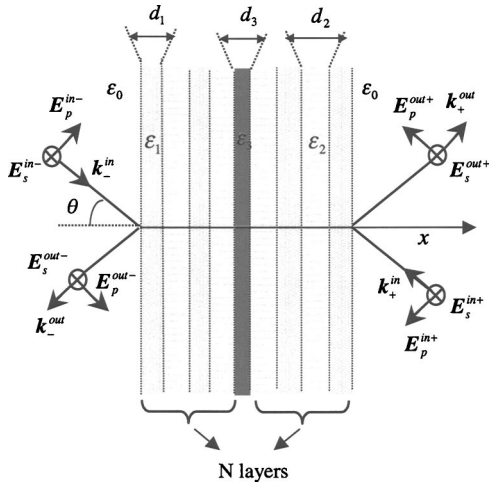

FIG. 1. Geometrical configuration of a single-defect Bragg stack (SDBS). The unit cell of a crystal consists of two lossless dielectric layers. The defect, symmetrically sandwiched between two identical crystals, has a loss dielectric layer.

[a)]Electronic mail: philippe.benabdallah@polytech.univ-nantes.fr

A. Hemispherical transmittance, reflectance, and absorptance

As we are interested in this work on spectral hemispherical radiative properties, we suppose the structure is irradiated on one side by a blackbody radiation. As the blackbody irradiance is isotropic and the problem has an azimuthal symmetry, the spectral hemispherical transmittance T_p (reflectance R_p and absorptance A_p, respectively) for TE or TM waves is therefore calculated by a simple integration of the directional spectral transmission t_p over the colatitude

$$T_p(\lambda) = 2\int_0^{\pi/2} t_p(\lambda,\theta)\cos\theta\sin\theta d\theta, \tag{2}$$

where p denotes the polarization status TE or TM and t_p is calculated from the transfer-matrix theory. [We have analog relations for the reflectance R_p and absorptance A_p. (In this case t_p must be replaced by the directional spectral reflection r_p and the directional spectral absorption a_p.) According to the energy conservation law (i.e., $A_p=1-T_p-R_p$) and Kirchoff's law[14] (i.e., the hemispherical emissivity ε_p is equal to A_p), we have $\varepsilon_p=1-T_p-R_p$. The unpolarized spectral hemispherical quantities are simply calculated by taking the arithmetical average of the polarized components.] In this framework the incoming and outgoing waves on both sides of the structure are linearly related by the following expression:

$$\begin{pmatrix} E^{\text{in}} \\ E^{\text{out}} \end{pmatrix}_p^- = \mathfrak{I}\begin{pmatrix} E^{\text{out}} \\ E^{\text{in}} \end{pmatrix}_p^+, \tag{3}$$

where

$$\mathfrak{I} = \left(\prod_{j=0}^{2N} T_{j,j+1}T_{j+1}^{\text{prop}}\right)T_{2N+1,0} \tag{4}$$

is the transfer matrix of the structure which is defined as the product of the interface transfer matrix

$$T_{ij} = \frac{1}{\boldsymbol{t}_{ij}}\begin{pmatrix} 1 & \boldsymbol{r}_{ij} \\ \boldsymbol{r}_{ij} & 1 \end{pmatrix}, \tag{5}$$

basically defined in terms of the Fresnel coefficients $\boldsymbol{t}_{ij}$ (transmission) and $\boldsymbol{r}_{ij}$ (reflection) and the propagation matrix

$$T_j^{\text{prop}} = \begin{pmatrix} e^{i\phi_j} & 0 \\ 0 & e^{-i\phi_j} \end{pmatrix}. \tag{6}$$

Here, ϕ_j stands for the phase shift of waves across the layer j. It follows that the transmission at the wavelength λ is defined from the field amplitudes or the transfer-matrix components as

$$t_p(\lambda) \equiv \left|\frac{E_+^{\text{out}}}{E_-^{\text{in}}}\right|^2_{E_+^{\text{n}}} = |\mathfrak{I}_{11}^{-1}|^2. \tag{7}$$

Figure 2 shows the calculation result of spectral hemispherical quantities of a single-defect Bragg stack (SDBS) composed of a silicon carbide (SiC) defect-layer thickness of 450 nm sandwiched between two identical four-cell periodic crystals. The unit cell of a crystal consists of a cadmium telluride (CdTe) layer of 1.2 μm and a germanium (Ge) layer of 760 nm. The crystal layers have an almost constant dielectric permittivity everywhere all over the range of investigation. In the absence of a defect layer no defect mode in the band-gap region is observed [dotted lines in Figs. 2(a) and

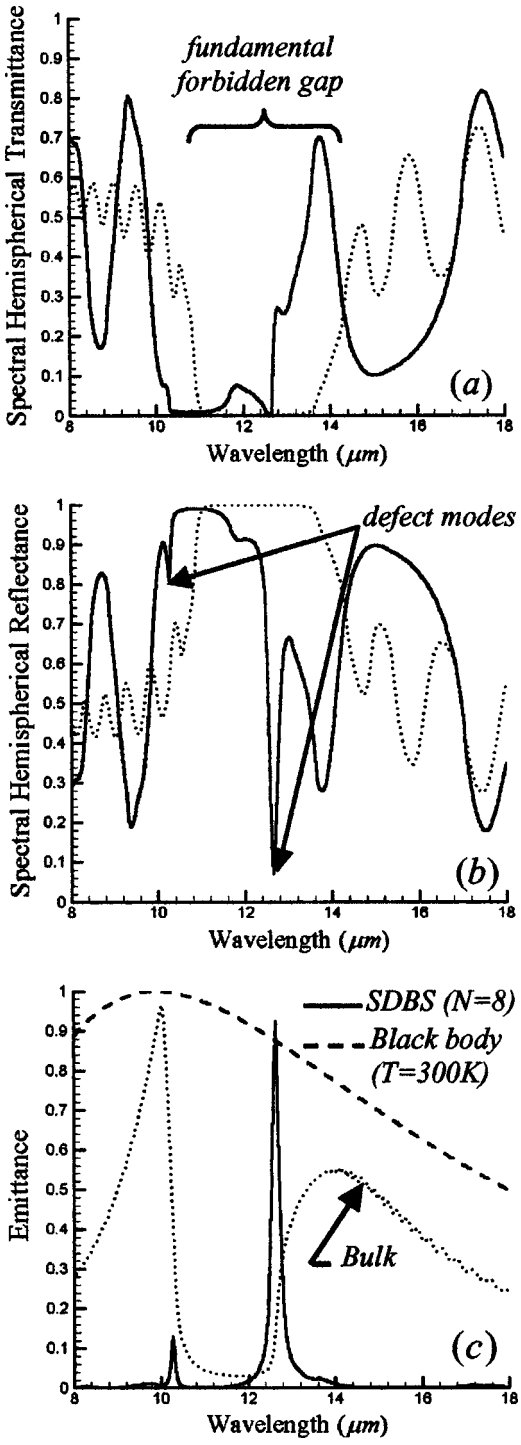

FIG. 2. (a),(b) Comparison between the spectral hemispherical transmittances (respectively, reflectances) of a pure (without defect) homogenized crystal (dotted line) and that of a SDBS below this regime (solid line). Numerical calculation has been carried out with $N=10$ layers (5 unit cells on each side of defect) in the first case and $N=8$ in the second one. The dielectric permittivity and related parameters are $\varepsilon_0=1$, $\varepsilon_1=7.29$, $\varepsilon_2=16$, $\omega_L=969\ \text{cm}^{-1}$, $\omega_T=793\ \text{cm}^{-1}$, $\Gamma=4.76\ \text{cm}^{-1}$, and $\varepsilon_\infty=6.7$, while each medium are assumed nonmagnetic ($\mu_1=\mu_2=\mu_3=1$). Computation have been done for the thickness $d_1=1.2$ μm, $d_2=760$ nm, $d_3=450$ nm. (c) Spectral hemispherical emittance. In dotted line is plotted the emittance of a massive SiC defect (100 μm) and in dashed line is represented the blackbody radiation (293 K), normalized by its value at the Wien's frequency.

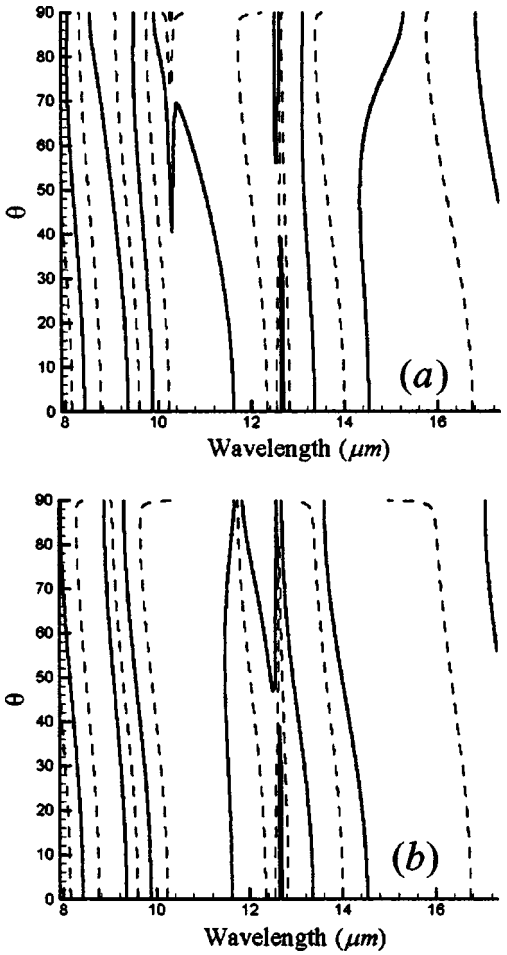

FIG. 3. Dispersion relations of resonant modes in (a) polarization *p* and in (b) polarization *s* for a SDBS with the same parameters as those used in Fig. 2. In dotted line is plotted the real part of the transcendental equation $\Im_{11}(\lambda,\theta)=0$, while in solid line is represented its imaginary part.

2(b)]. From $N=10$, the crystal reaches its homogenization regime and its spectral hemispherical transmittance does not change any more as the number of period increases. With the presence of the defect layer we see that two localized modes appear on the reflectance curve [Fig. 2(b)]. These peaks are comparable to the well-known donor modes we usually observe in semiconductors[10] when an extra dielectric material is added to unit cells. We note that these modes give quite different emission intensity. At $\lambda_1=10.3$ μm there is a low-power emission peak. As indicated by the dispersion relation of propagative resonant modes (Fig. 4), the peak is mainly the contribution of *p* waves. However, its magnitude seems too small (~ 0.1) to be used for practical applications.

On the other hand, at $\lambda_2=12.6$ μm we have a sharp emission peak with a much more stronger intensity. Unlike the former peak, which is located close to the band edge of the homogenized crystal, this one is located in the band-gap region of the crystal. More importantly, its intensity value is 0.93. It means that the emissivity of the structure is close to 1 for any angle between 0° and 90°. We also notice [Fig. 2(c)] that such an intensity drastically exceeds that of a single massive (100 μm) defect. Unlike the lower peak we see in Fig. 3, this peak results from both *p* and *s* waves. Note also that the high-power peak which occurs, for a blackbody radiation source at 293 K, beyond the maximum of the Planck function [Fig. 2(c)] will be obviously shifted toward the tail of the blackbody spectrum for higher temperatures and toward its head for lower temperatures.

B. Electric field distribution and defect-mode surface-mode coupling

For a better understanding of physical mechanisms that explain the optical behavior of SDBS we have further examined the field distribution inside the sample for different angles of incidence. In a preliminary step we calculate the reflectivity coefficient *r* of the whole sample. Then, the electric field on the right of the *k*th interface can be expressed as

$$E(x^{(k)},\lambda)=\frac{\Im_{22}^{(k)}+\Im_{21}^{(k)}-r(\lambda)\{\Im_{11}^{(k)}+\Im_{12}^{(k)}\}}{\det \Im^{(k)}}, \tag{8}$$

$\Im_{\mu\nu}^{(k)}$ being the elements of the transfer matrix from the first to the *k*th interface. The incoming field is normalized to 1. The intensity of the field inside the structure is then simply the square of the electric field, as plotted in Fig. 4. We see that the intensity inside the sample can become larger than 1 at several frequencies. This is attributed to internal resonances. The resonance pattern is strongly inhomogeneous over the spectrum throughout the sample. Close to 10 and 14 μm and in less important at 8.8 and 16.8 μm, we observe both at normal incidence and at oblique incidences the presence of some alleys of small resonance islands, where the intensity of field is superior to 1. Such a behavior is comparable to the well-known field enhancement in PBG materials,[15] close to the band edges. The likely first-order and second-order band-edge resonances are represented in Fig. 4 by horizontal dotted lines. More interesting here is the evolution of localized resonant sites at the two defect-mode frequencies (10.3 and 12.6 μm) as the period number of the crystal decreases. Indeed, while the magnification of the field at the band edge decreases with the period number of the crystal (these resonances disappear within the gap) the intensity of field at 12.6 μm (respectively, 10.3 μm) reaches a maximum (respectively, a minimum) value for $N=8$. This precisely corresponds to the emission patterns plotted in Fig. 6(a). Emission enhancement can be explained as the result of localized mode coupling. Indeed, as we can see in Fig. 4 the defect state at 12.6 μm is exponentially localized below the defect layer. There is also a resonance exponentially localized on the right of the air-crystal interface. This reveals the presence of a surface mode on this interface. Such a mode is a surface polariton, also called Fuchs–Kliewer[16] (FK) mode, which results, in this frequency range, from the atomic vibrations under the application of an electric field. As shown by the authors of Ref. 16, in a semi-infinite crystal and at the surface-polariton frequency, the local density of states (LDOS) oscillates close to the surface due to internal reflections of polaritons on this surface. Far enough from this region the polaritons "forget" the boundary and the LDOS naturally tends to that of a bulk crystal. For finite multilayered media with defects the situation is radically different because the surface polaritons coexist with localized defect modes. In a SDBS with enough number of layers, we see

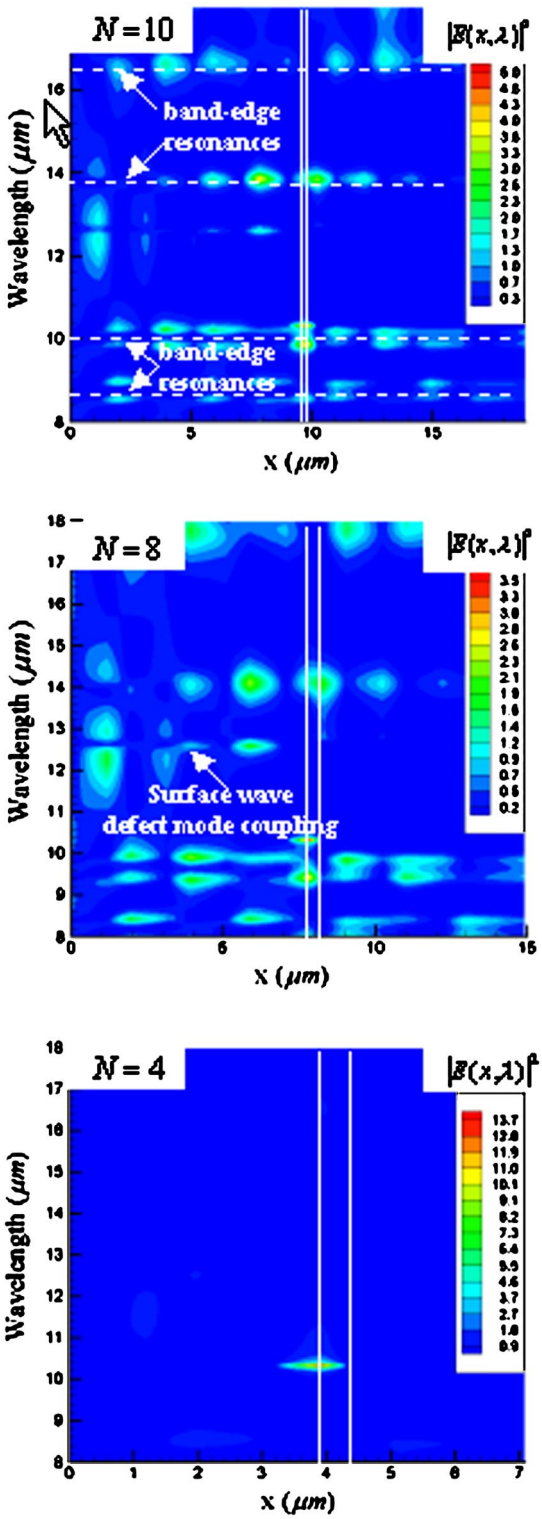

FIG. 4. (Color online) Calculated *x*-spatial distribution of the electric-field intensity inside a SDBS sample vs the period number *N* of crystal in polarization *p* at normal incidence. The physical parameters are those used in Fig. 2. The input intensity of the electric field has been normalized to unity. The intensity inside the sample can become larger than 1 due to internal resonances.

(Fig. 4, the $N=10$ case) that the surface and defect modes do not interact. However, contrary to a bulk crystal, such structures give rise to a sharp peak of emission (due to the presence of defect mode) with a relatively small magnitude. When the number of layer decreases, a coupling occurs (see

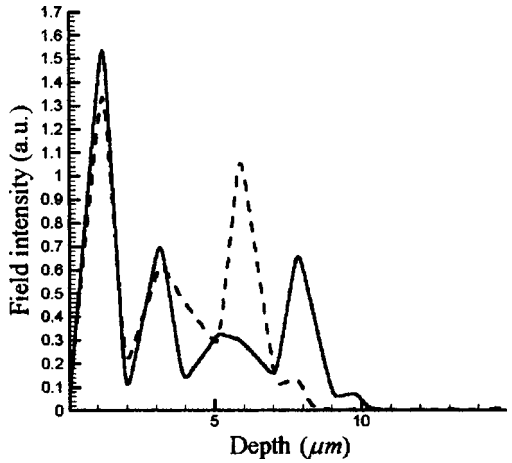

FIG. 5. Electric field distribution in a 10-layer SDBS (full line) and in an eight-layer SDBS (dashed line) at $\lambda=12.5$ μm.

Figs. 4 and 5, the $N=8$ case) between the surface and defect modes, and the thermal emission of the structure is notably enhanced. Moreover, the emission curve becomes narrowest (Fig. 6). In fact, we observe that the coupling effect magnifies (Fig. 5) the electric-field intensity at the defect-mode location, while the magnitude of the electric field close to the surface decreases in comparison with that of 10-SDBS (an analog behavior has been observed at oblique incidences). This coupling mechanism causes a decrease of reflectance and transmittance and leads to a strong absorption of light. Note also that, as we see in Fig. 6(a), the quality (Q) factor of the high-power emission peak is maximum for $N=8$. This can easily be understood with Fig. 4 since Q is determined by the effectiveness of the confinement in the x direction. When $N=8$, the coupling of the defect mode in the first-half part of the sample enhances significantly the energy confined in this direction compared with the other configurations, so that Q becomes maximum. Below a critical number of layers (Fig. 4, the $N=4$ case) the crystal band gap disappears and the magnification of fields induced by the confinement from band edges does not exist any more. As for the second defect mode at 10.3 μm, it is exponentially localized in both directions at the interface separating the crystal and the defect layer. Contrary to the other defect state, it does not couple with a surface mode so that most of its energy remains confined within the structure. When $N=10$, we also see that this defect mode resonantly couples with a band-edge mode. This and the weak absorption of SiC seem to explain why the emission is a little bit more intense at 10.3 μm. However, this coupling mechanism needs further investigations to be completely understood.

C. Sensitivity to defect parameters

The influence of the defect thickness and that of dielectric losses have also been analyzed. Comparing the curves plotted in Fig. 6(b), we observe that until a critical defect thickness, this critical value is about 45 nm. For visibility reasons, the corresponding emittance has not been plotted in Fig. 6(b). The augmentation of defect thickness simultaneously increases the magnitude and the linewidth of emis-

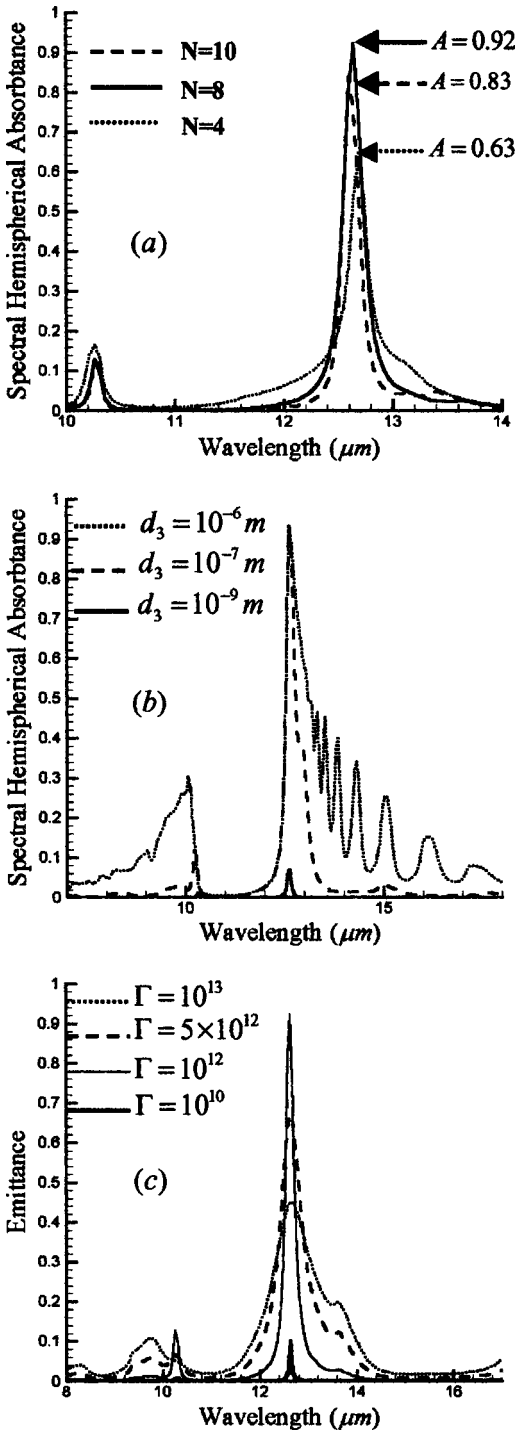

FIG. 6. Influence of (a) the crystal layer numbers, (b) the defect thickness, and (c) the dielectric losses on the spectral hemispherical absorptance of a SDBS. Γ is the damping parameter of the defect Lorentz model. The other physical parameters are the same as those used in Fig. 2.

sion peak. But from this critical thickness the emission saturates so that the *Q* factor, which is also defined as the center wavelength divided by the peak's linewidth, at last decreases. This is in good agreement with the experimental results of Lin *et al.*[17] Finally, we have discussed in Fig. 6(c) the role of the damping factor of the defect dielectric constant on the structure of emission spectrum. An increase in the absorption does not certainly magnify the emission but rather increases, from a critical absorption ($\Gamma \sim 10^{12}$), the linewidth of emission peak. Beyond this critical absorption, the absorptance of the structure drastically decreases and the peak of emission tends to disappear.

III. CONCLUSION

We have studied the radiative properties of Bragg stacks with plane absorbing defect embedded within. We found a regime below the homogenization regime of the crystal where it is possible to observe not only a narrow-band emission but also an emissivity close to 1 in all directions. This original behavior has been attributed to the coupling of defect states with surface modes. It has been demonstrated that this mechanism can be used to enhance thermal emission by extracting more energy of confined modes from the structure. Also, we have shown that the frequency and the *Q* factor of emission modes are tunable with the nature and size of the crystal and with the defect-layer properties. Finally, our numerical results have been shown to be in good agreement with previously published measurements.

Single-defect Bragg stacks could have a large impact on several technologies. For instance, they could be used to improve the efficiency of thermophotovoltaïc energy-conversion devices by limiting the heating of conversion cells due to the presence of photodissociation processes and the thermalization of electron-hole pairs above and below the frequency of conversion. Another promising application of SDBS is the field of IR spectroscopy and chemical sensing.

ACKNOWLEDGMENT

P.B.-A. thanks the French National Center for Scientific Research for financial support of this work.

[1] L. Mandel and E. Wolf, *Optical Coherence and Quantum Optics* (Cambridge University Press, Cambridge, England, 1995).
[2] R. Carminati and J.-J. Greffet, Phys. Rev. Lett. **82**, 1660 (1999).
[3] A. V. Shchegrov, K. Joulain, R. Carminati, and J.-J. Greffet, Phys. Rev. Lett. **85**, 1548 (2000).
[4] H. Sai, H. Yugami, Y. Akiyama, Y. Kanamori, and K. Hane, J. Opt. Soc. Am. A **18**, 1471 (2001).
[5] J. J. Greffet, R. Carminati, K. Joulain, J. P. Mulet *et al.*, Nature (London) **416**, 61 (2002).
[6] K. Richter, G. Chen, and C. L. Tien, Opt. Eng. **32**, 1897 (1993).
[7] S. John, Phys. Rev. Lett. **58**, 2486 (1987). Also, see E. Yablonovitch, Phys. Rev. Lett. **58**, 2059 (1987). For a more recent review, see H. Benisty, S. Kawakami, D. Norris, and C. Soukoulis, *Photonics and Nanostructures : Fundamentals and Applications* (Elsevier, New York, 2003).
[8] M. U. Pralle *et al.*, Appl. Phys. Lett. **81**, 4685 (2002).
[9] L. McCall, P. M. Plazman, R. Dalichaouch, D. Smith, and S. Schultz, Phys. Rev. Lett. **67**, 2017 (1991).
[10] E. Yablonovitch, T. J. Gmitter, R. D. Meade, K. D. B. A. M. Rappe, and J. D. Joannopoulos, Phys. Rev. Lett. **67**, 3380 (1991).
[11] M. M. Sigalas, C. M. Soukoulis, C. T. Chan, R. Biswas, and K. M. Ho, Phys. Rev. B **59**, 12767 (1999).
[12] M. Iida *et al.*, Phys. Rev. B **69**, 245119 (2004).
[13] M. M. Sigalas, K. M. Ho, R. Biswas, and C. M. Soukoulis, Phys. Rev. B **57**, 3815 (1998).
[14] M. F. Modest, *Radiative Heat Transfer* (McGraw-Hill, New York, 1993).
[15] I. Bulu, H. Caglayan, and E. Ozbay, Phys. Rev. B **67**, 205103 (2003).
[16] A. Dereux, J. Vigneron, P. Lambin, and A. A. Lucas, Phys. Rev. B **38**, 5438 (1988).
[17] S. Y. Lin, V. M. Hietala, S. K. Lyo, and A. Zaslavsky, Appl. Phys. Lett. **68**, 3233 (1996).